Progress towards picosecond on-chip magnetic memory

Abstract

We offer a perspective on the prospects of ultrafast spintronics and opto-magnetism as a pathway to high-performance, energy-efficient, nonvolatile embedded memory in digital integrated circuit applications. Although conventional spintronic devices, such as spin-transfer-torque-based MRAMs (STT-MRAM), are now commercially demonstrated, they are limited in write speed to the nanosecond timescale. Improvement in the write speed of spintronic devices can significantly increase their usefulness as viable alternatives or complements to existing CMOS-based devices with intrinsic switching speeds on picosecond timescales. In this article, we discuss recent studies which advance the field of ultrafast spintronics and opto-magnetism. An optimized ferromagnet-ferrimagnet (FM-FEM) exchange-coupled magnetic stack, which can serve as the free layer of a magnetic tunnel junction (MTJ), can be optically switched in as little as ~3 ps. Integration of ultrafast magnetic switching into an MTJ device has enabled electrical readout of the switched state using tunneling magnetoresistance (TMR) with a high resistance ratio. Purely electronic ultrafast spin-orbit torque (SOT) induced switching of a ferromagnet has been demonstrated using ~6 ps pure charge current pulses. We conclude our perspective by discussing some of the challenges that remain to be addressed to advance ultrafast spintronics technologies toward practical implementation in high-performance digital information processing systems.

Introduction

With the advent of massive data-intensive artificial intelligence algorithms, on-chip memory is becoming increasingly important in modern computing systems. However, in the conventional silicon CMOS-based random-access memory (RAM) devices (static and dynamic RAM, i.e. SRAM and DRAM), there exist challenges in the form of volatility, active/passive energy dissipation, and scalability which become more difficult with reduced feature size[1–7]. The field of spintronics is emerging as a promising alternative technology that utilizes the spin degrees of freedom of the electron instead of just its charge for data manipulation. The non-volatility of magnetic bits in spintronic devices results in low static energy dissipation and enables efficient fine-grained processor power management approaches, leading to improved overall system energy efficiency. Additionally, they have other desirable properties such as high endurance and relative ease of integration with existing Si processes.

The state-of-the-art among conventional spintronic devices is the *magneto-resistive* random-access memory (MRAM). The building block of an MRAM device is a magnetic tunnel junction (MTJ) which consists of two ferromagnetic layers separated by a thin oxide tunnel barrier layer. One of the ferromagnetic layers constitutes a fixed reference and its magnetization remains unchanged over the operation of the device. The second ferromagnetic layer is called the "free layer" and its magnetization can be flipped to store either a 0 or a 1 of binary information. The reading of the magnetization state of the device is performed by passing a small current across the MTJ device and measuring the tunneling magnetoresistance (TMR) of the memory cell which is known to depend on the relative orientations of the free and reference layers. With increasing TMR ratio between the two resistance states, the reading operation can be performed with higher accuracy and with smaller and faster reading current[5].

First versions of MRAM used in-plane magnetized thin films and were written via the Oersted fields generated by the currents circulating through the addressing wires[8,9]. Newer versions exploit the faster, more energy-efficient, and scalable spin-transfer torques (STT) and spin-orbit torques (SOT) in order to control the magnetization of out-of-plane magnetized materials[1,2,5,9–11]. Schematic representations of STT and SOT pulse-induced switching mechanisms in a MTJ framework are shown in Fig. 1a,b. STT arises due to the transfer of spin angular momentum between two adjacent non-collinear magnetized layers[5,12]. In STT-MRAM devices (as schematically shown in Fig.1a), a large write charge current is passed across the thickness of the MTJ cell. It leads to a flow of spin-current and the transfer of angular momentum from the reference (or pinned) layer to the free magnetic layer which ultimately reverses the magnetization direction of the free layer. The switching time of STT-MRAM devices ranges from a few ns to tens of ns depending on the write current density and pulse width. Reliable 2-3 ns switching of STT-MRAM devices have been demonstrated with less than 10^{-6} write error rate (WER)[13,14] showing bright prospects for its use in "last-

level" on-chip memory caches[15,16]. Industrial partners have already demonstrated several standalone and embedded working STT-MRAM devices[17–19]. However, STT devices require that a relatively high write current density must be passed through the oxide tunnel barrier which, after many cycles, degrades the oxide quality and ultimately limits the endurance of the device. Another drawback of the STT device is the incubation delay resulting in a wide distribution of switching times,[15,20,21] even in a single junction.

An alternative to STT-MRAM is to use the SOT mechanism. SOT originates either i) at the interface of the magnetic and the non-magnetic metal due to the interaction of spin-orbit coupling, magnetic exchange, and symmetry breaking at the interface which can be interpreted with the Rashba-Edelstein effect[12,22–24] or ii) due to the flow of spin currents from the non-magnetic metal to the magnetic layer which can be explained by spin-Hall effect[25–27]. In SOT-MRAM devices, a charge current is passed through a heavy metal (typically Ta, Pt, or W) wire (as schematically shown in Fig.1b), which leads to a transverse spin current, causing a spin accumulation at the surfaces and interfaces of the heavy metal wire (as schematically shown in Fig.1b). The accumulated spins can then exert a torque (called the spin-orbit torque) on the spins in an adjacent magnetic film, for example, the free layer of an MTJ. SOT-MRAM devices are faster (sub-ns to few ns)[28–32] and can be energy-efficient[6,27,33] than STT-MRAM devices, and offer increased endurance as the write current only needs to pass through the heavy metal layer, and not through the tunnel barrier layer in the MTJ. SOT-MRAM has found applications as L1/L2 SRAM cache replacement[15], although being a three-terminal device, the density of MRAM may be lower compared to STT-MRAM or conventional SRAM and DRAMs. STT-MRAM and SOT-MRAM devices have the potential to be used instead of conventional SRAM and DRAM devices due to their advantages of low switching energy, faster speed, non-volatility, and nanoscale integration[1–3,6]. The typical writing energy densities (per unit area) of STT and SOT-MRAM devices are ~40 aJ/nm^2 and ~1 aJ/nm^2 respectively[6]. A significant disadvantage of these spintronic devices compared to CMOS devices is the write speed. Ferromagnetic materials at thermal equilibrium are limited in switching speed by their precessional dynamics, which is typically in the GHz frequency range[34–37]. The fastest reported STT and SOT device required ~50 picoseconds (ps)[38] (for in-plane magnetized sample) and ~200 ps[27] current pulses respectively. It is highly desirable to increase the magnetization switching speed significantly so that the spintronic devices can be more competitive with CMOS-based devices.

To improve the switching speed of magnets in spintronic devices we turn to the field of ultrafast magnetism (or femtomagnetism), which was discovered in 1996 by Bigot and Beaurepaire[39] with the observation of sub-ps magnetization quenching of a ferromagnetic Ni thin film upon irradiation with ultrafast laser pulses. Their work first demonstrated that femtosecond (fs) laser pulses could be used instead of external magnetic fields to manipulate the magnetization state of a material in an ultrafast fashion. Ultrafast manipulation of magnetization using femtosecond optical pulses is of particular interest as the magnetization dynamics are much faster than conventional precessional dynamics. The most exciting phenomenon in ultrafast

magnetism is arguably the ultrafast helicity independent all-optical switching (HI-AOS)[40–42] of magnetization, wherein a magnetic film reverses its magnetization (and not just demagnetizes) within a couple of ps by a single ultrashort (~100 fs) laser pulse irradiation. Ultrafast HI-AOS does not require an external magnetic stimulus, is independent of the polarity (helicity) of the laser pulse, and is understood to be arising from the ultrafast non-equilibrium heating of the magnet by the laser pulse[41–45]. This phenomenon was reported first in GdFeCo alloy[40] in 2011 and then mainly in other Gd-based alloys and multilayers (MLs)[41,46–52] with a few interesting exceptions such as Mn_2Ru_xGa alloy[53] and Co/Tb ML[54–56]. In all of these cases, the magnetic material is ferrimagnetic, rather than ferromagnetic. Another surprising feature of HI-AOS is that the magnetization switches back and forth upon subsequent laser pulses in a "toggle" switching fashion.

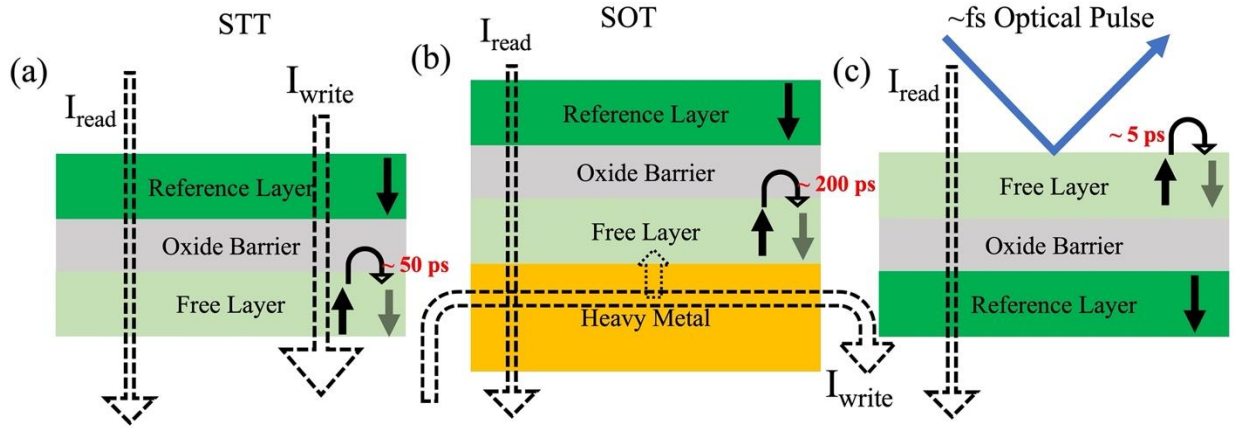


Figure 1: The schematic of a basic MTJ cell employing (a) STT, (b) SOT mechanism, and (b) femtosecond pulse excitation

Instead of using a conventional ferromagnet as the free layer of the MTJ building block, researchers have studied a toggle-switchable ferrimagnet exhibiting HI-AOS as the free layer. The free layer in such an opto-spintronic device is switched optically and then the TMR across the MTJ is measured to read the corresponding magnetization state[54,55,57,58]. However, the TMR ratio of an MTJ device tends to be small when only a ferrimagnet is used as the free layer[57] due to its low spin-polarization. Unfortunately, according to the current understanding of the HI-AOS mechanism, a conventional ferromagnetic free layer (with larger TMR) cannot be switched optically. However, recent experiments have shown that a ferromagnetic free layer which is exchange-coupled[59,60] with an optically switchable ferrimagnet, can be utilized to switch the free layer i.e. the ferromagnet. A ferromagnet layer can also be switched via laser-induced spin-current generated from the ultrafast demagnetization of an optically switchable ferrimagnet[61–63]. Such switching magnetic bilayers can then be utilized to enhance the TMR in an MTJ device.

In Section 1 of this perspective, we review our recent experimental observations of magnetization reversal dynamics of a ferromagnetic Co/Pt ML coupled to a ferromagnetic $Co_{70}Gd_{30}$ alloy which can be used as the free layer of an opto-MTJ stack. We explain the ultrafast HI-AOS of the Co/Pt using an extended microscopic three temperature model (M3TM)[34,43,47,64,65] and show that an indirect Ruderman–Kittel–Kasuya–Yosida (RKKY) exchange interaction between the Co/Pt and CoGd[66,67] can explain the switching of the ferromagnet in ultrafast timescale. In Section 2, we review studies of optical switching of a complete opto-MTJ cell, the free layer of which comprises a consisting of a read and write junction (optically switchable ferrimagnet coupled with a ferromagnet) separated by a thin oxide barrier layer. In one of those studies, the authors investigated the ultrafast time-resolved magnetization reversal dynamics of an MTJ, which is a substantial stride towards building a functional opto-MRAM device. In the last section, we discuss one of our recent studies where we observe ultrafast SOT induced magnetization reversal in a Co thin film using ~6 ps electrical pulse from an ultrafast photo-conducting "Auston switch"[68] in the presence of a symmetry-breaking in-plane magnetic fields. Time-resolved measurements in the low (sub-switching) fluence domain confirm the effect of damping-like torque and field-like torque for different in-plane magnetic field and ultrafast current directions. We discuss the switching mechanism using a temperature-dependent Landau-Liftsitz-Gilbert (LLG) macro-spin model. Finally, we conclude this review by addressing some challenges of designing advanced spintronic devices based on the combination of HI-AOS and SOT. We also discuss our perspective on the future developments in this field.

Section 1: Ultrafast all-optical magnetization switching of a ferromagnet in a coupled ferromagnet-ferrimagnet heterostructure

As mentioned previously, one idea for building an opto-spintronic device is to use an optically switchable ferrimagnet as the free layer of an MTJ and electrically read the magnetization state by measuring the TMR. The TMR of an MTJ is much higher with a conventional ferromagnet layer on both sides of the oxide barrier due to their high spin-polarization[54,55,69,70], and the enhanced TMR improves the reading speed and read distribution rate of an MTJ[71]. We previously investigated the magnetization dynamics of a Co/Pt layer exchange-coupled via RKKY interaction with a GdFeCo alloy to use it as a free layer of an MTJ cell[60]. The nature of the RKKY exchange coupling was tuned by simply changing the thickness of a metallic spacer layer (Pt in our case) between the two magnetic layers. We showed that the Co/Pt layer, coupled either ferromagnetically or anti-ferromagnetically with the GdFeCo alloy, can be switched in ~7 ps upon irradiation by a short laser pulse[59]. However, we separately have observed that a GdFeCo film does not maintain perpendicular magnetic anisotropy (PMA) below lateral dimensions of 1 μm, whereas CoGd

retains its PMA even for ~200 nm dot size[48]. Scaling these magnetic bits to sub-100 nm lateral dimensions with PMA is critical for achieving high device density.

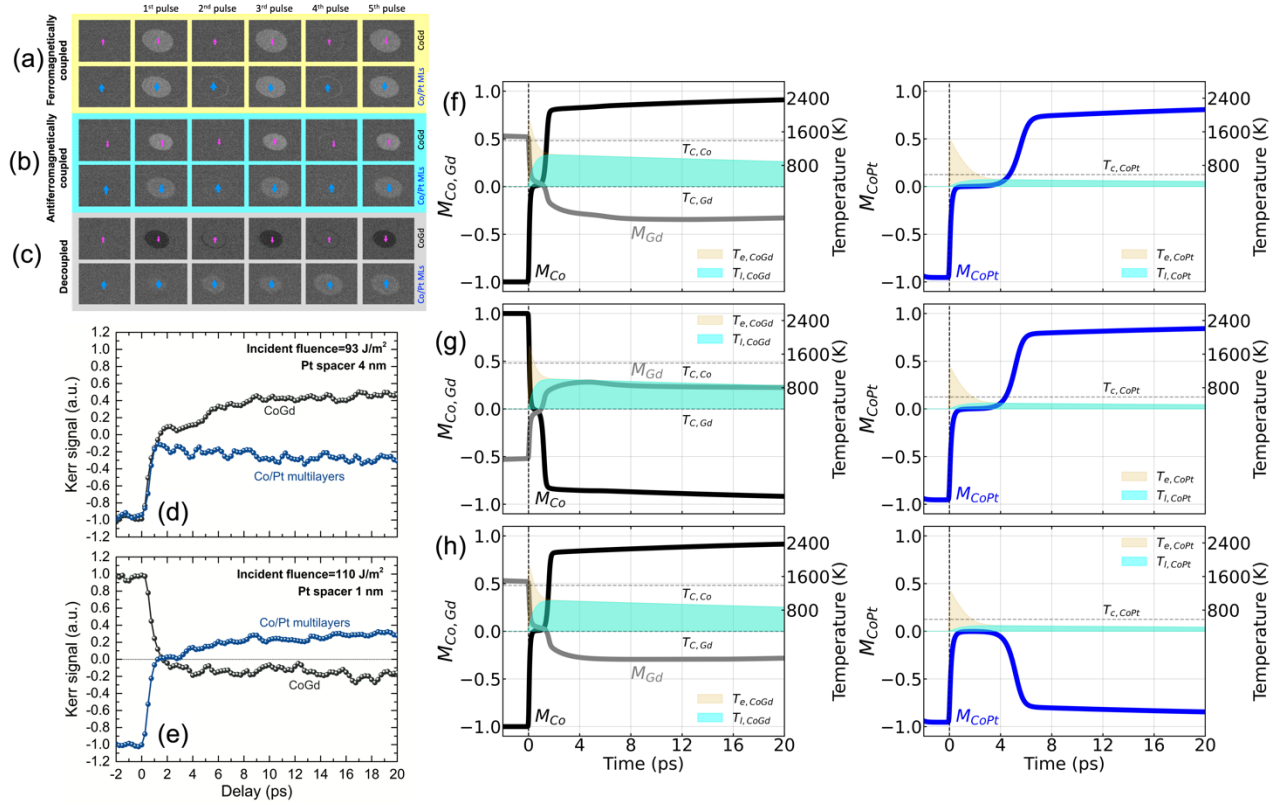


Figure 2: (a-c) Depth sensitive single-shot MOKE micrographs of the (a) ferromagnetically, (b) anti-ferromagnetically and (c) decoupled FM-FEM stack. (d-e) Depth-sensitive time resolved magnetization dynamics of Co/Pt and CoGd for decoupled (d) and ferromagnetically coupled (e) stacks. (f-h) The simulated magnetization dynamics of Co, Gd, and Co/Pt sublattice simulated for ferromagnetically, anti-ferromagnetically and decoupled FM-FEM stack and the time-evolution of corresponding electron and lattice temperature using the extended M3TM model and the corresponding evolution of electron and phonon temperatures are shown by light yellow and cyan filled regions, respectively, and the Curie temperatures of Co and Co/Pt are shown by the dotted lines as taken from[60]. Reprinted with permission from the authors.

Hence, we also studied the HI-AOS dynamics of a Co/Pt layer when exchange coupled to $Co_{70}Gd_{30}$ alloy via RKKY type exchange interaction[60]. The complete structure is the following: Substrate/Ta_3/Pt_2/$[Co_{0.5}/Pt_{0.25}]_{x3}$/$Co_{0.5}$/$Pt_d$/$CoGd_{10}$/$Pt_3$, where the thicknesses of the layers in nm are given as subscripts and the Pt spacer layer has variable thickness *d* for different samples. The RKKY coupling was tuned from ferromagnetic (d: 1, 1.5 and 2 nm) to anti-ferromagnetic (*d*: 2.5 and 3 nm) to decoupled (*d*: 3.5 and 4 nm) by changing the Pt spacer layer thickness (*d*) from 1 to 4 nm. We found the exchange bias of the antiferromagnetically coupled stacks to be 1160 Oe and 100 Oe respectively for 2.5 and 3 nm Pt by performing minor hysteresis loops of CoGd[60]. Depth-resolved single-shot HI-AOS MOKE micrographs, obtained using the layer-sensitive MOKE measurement technique[59,72,73], are shown in Fig. 2a-c for different

Pt layer thicknesses. Using this technique, we can distinguish the magnetization of the CoGd and Co/Pt layers separately by carefully tuning the angle of a $\lambda/4$ plate in the light path. For ferromagnetically and anti-ferromagnetically coupled stacks, as shown in Fig. 2a-b, the magnetizations of both the CoGd layer and Co/Pt layer (respectively represented by pink and blue arrows) get switched with successive single-shot laser pulses as observed from the change in magnetic contrast where the pulse energy is higher than the switching threshold. However, when the layers are decoupled, as shown in Fig. 2c, only the CoGd demonstrates toggle switching but CoPt stays demagnetized as evident from the reduced magnetic contrast, and the magnetization direction is shown with the unidirectional blue arrow. Non-local spin-current coming from the demagnetization of the Gd sublattice has been argued to be the reason for the ultrafast switching of Co/Pt in magnetic heterostructures where the ferromagnet (Co/Pt) is separated from the optically switchable ferrimagnet[61–63] with thick Cu layer (~10 nm). The thick Cu layer denies any magnetic coupling between the two layers. In our structure, the Pt spacer is 3 nm thick for the antiferromagnetically coupled stack and more importantly, the magnetization of Co/Pt ML switches for both parallel and anti-parallel alignment with CoGd, which proves that switching of Co/Pt ML is mediated by RKKY exchange coupling ruling out the role of non-local spin current in the switching of the Co/Pt ML. Layer-resolved single-shot switching experiments demonstrate the dynamics of the switching phenomenon in CoGd and Co/Pt MLs as shown in Fig. 2d-e. In the decoupled stack (Fig. 2d), CoGd switches (crosses zero) in ~1.5 ps, and the Co/Pt gets demagnetized close to ~90 % before showing a slow remagnetization towards its initial magnetization direction. For the ferromagnetically coupled stack (Fig. 2e), CoGd reverses its magnetization after ~1.5 ps. The Co/Pt ML exhibits a two-step like switching i.e. an almost complete demagnetization in ~450 fs (due to ultrafast optical excitation/heating) and magnetization reversal in ~3 ps (because of angular momentum exchange with the already reversed CoGd). Such a two-step process strongly supports that the RKKY exchange interaction is responsible for the reversal of already softened (hot) Co/Pt magnetization. This is the fastest reported switching of a ferromagnet irrespective of the stimuli (STT, SOT, or AOS) to the best of our knowledge.

We model the observed RKKY exchange coupling mediated ultrafast AOS by extending the M3TM proposed by Beens *et al.*[43,65,74]. We consider (i) an inter-sublattice exchange scattering between Co and Gd, (ii) a long-range RKKY exchange between the Co and Gd sublattices of CoGd and Co/Pt, and (iii) the Elliot-Yafet type spin-flip scattering for the CoGd and Co/Pt subsystems. Our simulations show that the reversal of CoGd for three types of stacks occurs at ~1.5 ps. There are no large differences observed in CoGd reversal dynamics for ferromagnetically, antiferromagnetically coupled, and decoupled stacks, which are shown in Fig 2f-h. On the other hand, a clear difference is observed for the magnetization dynamics of Co/Pt between decoupled and coupled samples. The electron temperature of Co/Pt increases beyond its Curie temperature for a sufficiently high absorbed laser fluence. As a result, Co/Pt stays demagnetized until

it cools down and is acted on by the RKKY exchange from the already switched CoGd, leading to the two-step switching. We observe that the switching time of Co/Pt strongly reduces with increasing RKKY exchange strength for a fixed laser fluence. It has been shown that Co/Pt cannot be switched for a decoupled stack where there is no angular momentum transfer channel between the two subsystems by exchange coupling, whereas, for the magnetically coupled stack, the Co/Pt can be switched in ~4 ps even if the RKKY exchange scattering strength is only ~5% of the direct exchange of CoPt as shown in Fig. 2f-h. The range of RKKY coupling used in the simulation is $J_{RKKY} = \pm 0.05 * J_{CoPt} = \pm 6.658 \times 10^{-23}$ J. If we assume a typical lattice constant of 4Å (a), the coupling strength (J/a^2) becomes $\pm$ 0.416 mJ/m^2. S. S. P. Parkin[75] measured exchange coupling strength of various 3d, 4d, and 5d transition metals at room temperature and found a variation of RKKY-type exchange coupling from 0.1 to 10 erg/cm^2. Our estimated values remain well within the range of Parkin's measured values.

The experimental observations confirm the ultrafast switching of the Co/Pt layer within ~3 ps in an FM-FEM exchange-coupled heterostructure and is an important step towards the practical realization of an ultrafast memory. The theoretical analysis demonstrates that RKKY exchange alone can trigger such an ultrafast switching without the need of any spin current.

Section 2: Ultrafast magnetization dynamics in an MTJ device

After the first observation of HI-AOS in GdFeCo in 2011[40,41], such ultrafast switching has been studied in a plethora of magnetic systems such as CoGd, GdTbCo, Co/Tb, Gd/Co, and Mn_2Ru_xGa[43,45,48–50,53–56,76]. The first HI-AOS in an MTJ cell was reported in 2017 by Chen *et al.*[57], where the authors employed an optically switchable $Gd_{26}(Fe_{90}Co_{10})_{74}$ layer as the free layer and a Co/Pd ML coupled to another Co layer as the reference layer of the MTJ cell. They used 100-nm-thick Indium Tin Oxide (ITO) electrodes for the top contact which offer better laser-pulse access and electrical detection compared to commonly used Ti/Au electrodes. The authors fabricated a 12 μm diameter MTJ device, schematically shown in Fig. 3a, with the following stack configuration: $Ta_5/Pd_{10}/(Co_{0.6}/Pd_{1.5})_{x3}/Co_{0.8}/MgO_{1.8}/GdFeCo_{20}/Ta_4$, and MgO is the oxide barrier layer. The electrical read-out of the HI-AOS of $Gd_{26}(Fe_{90}Co_{10})_{74}$ free layer of the MTJ cell was performed by measuring TMR of the memory cell, which is shown in Fig. 3b. A small TMR ratio (~0.6 %) was observed due to the low quality of the MgO barrier and low spin polarization of the ferrimagnet. The signal-to-noise ratio (SNR) was low due to the degraded interface qualities between the ITO and Ta/GdFeCo layers. They demonstrated the repeatability of AOS in GdFeCo Hall devices with measurements at a 1 MHz repetition rate. The fundamental upper limit of the switching rate should be higher than tens of GHz, however, the actual switching speed wasn't measured. This experiment was a substantial step towards realizing a working opto-spintronic device that directly converts ultrafast optical

signals to non-volatile magnetic states. They mentioned that larger TMR, improved SNR, a stable PMA with reduced device size, and smaller critical fluence are required for large-scale integration and practical application. However, as we have discussed in Section 1, GdFeCo alloys have the difficulty of maintaining PMA when patterned to less than a micron diameter[48], hence it is not ideal for device applications. In 2020, Avilés-Félix *et al.*,[55] developed an optically switchable CoFeB-$[Tb/Co]_N$ exchange-coupled heterostructure. First, they systematically studied the magnetic and HI-AOS properties of a $[Tb/Co]_5$ layers by continuously varying the thickness of Co and Tb in the range of 0.6 nm < t_{Tb} < 1.6 nm and 0.7 nm < t_{Co} < 1.4 nm after annealing at different temperature[54]. Several previous studies reported the degradation of anisotropy for such optically switchable films with annealing temperature which hinders their technological application[77,78].

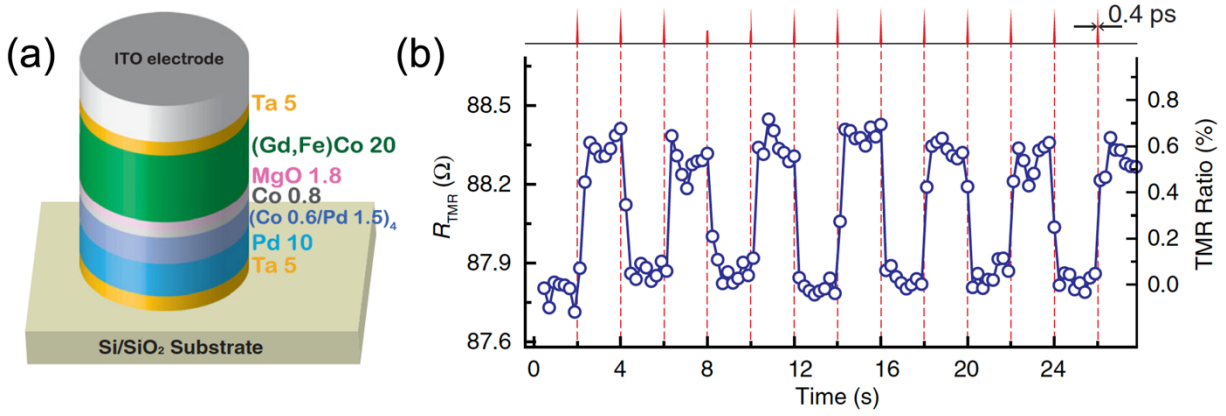


Figure 3: (a) Schematic of the MTJ stack employing $Gd_{26}(Fe_{90}Co_{10})_{74}$ as the free layer and Co/Pd ML as the reference layer, (b) HI-AOS of the 12 mm MTJ cell measured via TMR electrical read-out as reproduced with the permission from Chen *et al.*,[57] copyright 2017 AIP Publishing.

However, in a recent study, it was reported that although the anisotropy of a Co/Gd bilayer reduced with increasing annealing temperature, HI-AOS properties became more energy efficient, and the domain-wall velocity increased[79] due to enhanced intermixing at the Co/Gd interface. Studying the dependence of the coercivity and PMA on the annealing temperature ranging from 200 to 300 C, Avilés-Félix *et al.*[55] found that the coercivity of a $[Tb_{1.0}/Co_{1.2}]_5$ ML reduced sharply with increasing annealing temperature and this reduction strongly depended on the ratio of t_{Co}/t_{Tb} (ratio of thicknesses of Co and Tb). The weakening of the static magnetic properties was attributed to the enhancement of the interfacial roughness originating from interdiffusion or structural relaxation. They studied HI-AOS properties of the half-MTJ stack comprising Seed layer/MgO/$CoFeB_{1.3}$/$Ta_{0.2}$/$[Tb(t_{Tb})/Co(t_{Co})]_5$ (annealed at 250^0 C) with varying Co and Tb layer thicknesses using both ~60 fs and ~5 ps laser pulses. Single-shot HI-AOS was observed for half-MTJ stacks with relatively thicker Co than the Tb layer as shown in Fig. 4 a, b. They observed that either ~60 fs

and ~5 ps pulses could switch CoFeB-$[Tb_{0.8}/Co_{1.2}]_5$ and CoFeB-$[Tb_{1.0}/Co_{1.3}]_5$, however, HI-AOS in CoFeB-$[Tb_{1.1}/Co_{1.3}]_5$ was observed with only 5 ps pulses. They integrated their optically switchable half-MTJ into an MTJ cell with the following structure: $Ta_{0.3}/CoFeB_{1.1}/MgO/CoFeB_{1.2}/Ta_{0.2}/[Tb/Co]_N$, where $FeCoB_{1.1}$ served as the sensing layer. They fabricated 0.94 nm-thick and 1.8 nm-thick MgO barriers for N = 15 and 5 repetitions of the [Tb/Co] bilayers and nano-patterned those with the dot diameter varying from 50 nm to 200 nm. In the supplementary information of Félix *et al.*[55], the critical fluence of HI-AOS of the $[Tb_{1.0}/Co_{1.3}]_5$ ML in the MTJ cell decreased with increasing laser pulse-width. This was a surprising observation as we generally observe an enhancement of the critical switching fluence for longer pulses in FEM alloys[50,80]. A TMR ratio of ~38 % and ~28 % TMR for N = 15 and 5 repetitions of the [Tb/Co], respectively, was reported[55] as shown in Fig. 4c. The detected TMR value is much larger than the ~0.6 % TMR observed by Chen *et al.*[57], and it is stable even after nano-structuring and annealing. Hence, the MTJ cells with optically switchable CoFeB-$[Tb/Co]_N$ free layers, seem to be a promising candidate for integration within hybrid opto-spintronic devices. Experiments are ongoing to measure the HI-AOS properties of these nano-pillar MTJs as a function of dot diameter and laser fluence.

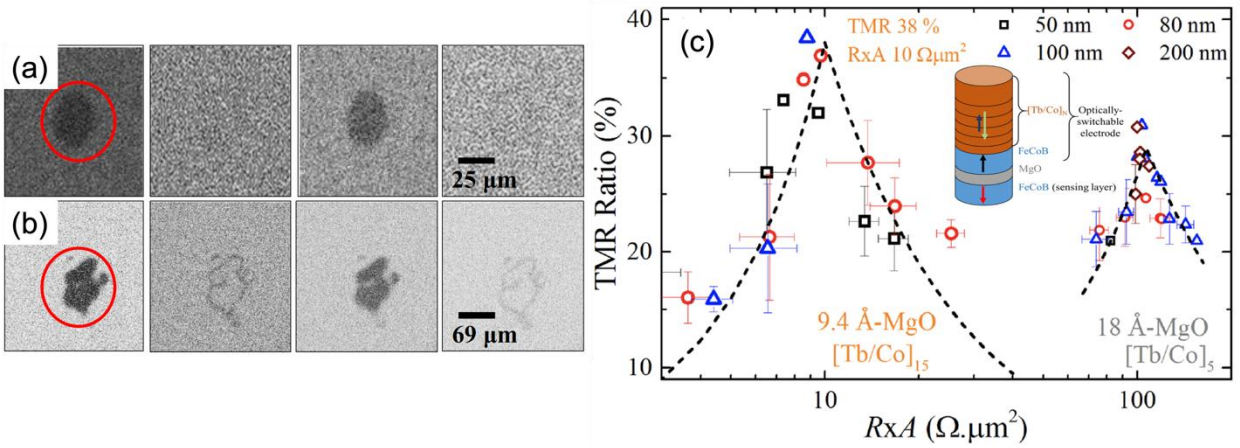


Figure 4: MOKE micrograph of the half-MTJ stack (CoFeB/Ta/$[Tb_{1.0}/Co_{1.3}]_5$) as observed with a (a) 5 ps and (b) 60 fs single-shot laser pulse and (c) TMR ratio of the full MTJ stack for two different MgO barrier layer thickness and with varying device size from 50 nm to 200 nm and the schematic of a half-MTJ and full MTJ stack employing CoFeB-$[Tb/Co]_N$ as the optically switchable layer and another CoFeB as the reference layer is shown at the inset. Reproduced with permission from Félix *et al.*,[55] copyright 2020 Nature Publishing.

The time-resolved magnetization dynamics of an exchange coupled FM-FEM heterostructure as a free layer of a micron-sized MTJ cell was reported recently by Wang *et al.*[58], where they observed for the first time that the ultrafast switching occurs in 10 ps for a 3 µm MTJ dot diameter. The authors used DC and RF sputtering to fabricate an opto-MTJ structure consisting of: $Substrate/Ta_3/Ru_{20}/Ta_{0.7}/[Co/Pt]_{9.8*m}/Ru_{0.8}/[Co/Pt]_{3.6*n}/Ta_{0.3}/CoFeB_{1.2}/MgO/CoFeB_1/Ta_{0.3}/Co_1/Gd_3/Pt_2$. Here, Ta/Ru/Ta served as the bottom electrode, $[Co/Pt]_{m/n}$ MLs with the bottom CoFeB served as the

synthetic antiferromagnetic (SAF) reference layer (RL), and the optically switchable free layer consisted of a top CoFeB layer exchange coupled with the Co/Gd ferrimagnetic bilayer. They structured their MTJ down to 3 μm dot size and measured a TMR ratio of ~34% upon annealing their MTJ cells at 300^0 C. The magnetization of the free layer toggled between parallel (P) and antiparallel (AP) states with respect to the magnetization of the RL due to HI-AOS, when the patterned cells were exposed to a series of single-shot ultrafast laser pulses. They explored the magnetization reversal dynamics of the free layer of the MTJ stacks using time-resolved MOKE measurements starting from each of the two oppositely orientations of the free layer (shown in blue and black) of the MTJ. They demonstrated a zero crossing of the magnetization of the free layer at ~5 ps, with complete switching taking ~200 ps. The switching was attributed to ultrafast heat-induced demagnetization of the antiferromagnetically coupled Co and Gd layers, and the exchange scattering-mediated angular momentum transfer between them. They measured the switching dynamics of the MTJ cell with its diameter varying from 3 to 10 μm. The switching time in this work was defined by the time needed to reach 75% of saturation of the opposite magnetization[48]. The observed switching time varied from 10 ps to 40 ps for device sizes varying from 3 μm to an unpatterned layer. The observed scaling of the switching time with the MTJ dot diameter is similar to our previously reported switching in CoGd alloy dots and was explained by enhanced surface-mediated heat transfer in smaller dots[48], due to the increased electron-phonon coupling at smaller size[81].

These proof-of-concept studies provide the experimental demonstration of optically toggle-switchable MTJ stacks and demonstrate the time-resolved switching dynamics of a micron-sized MTJ cell showing the ultrafast magnetization reversal in tens of ps timescales. The switching time of the MTJ free layer is similar to standalone FEM dots[48]. These measurements serve as an essential milestone towards the development of large-scale opto-spintronic arrays.

Section 3: Spin-orbit torque induced ultrafast magnetization switching in a ferromagnet

In 2017 we demonstrated a new method to control the magnetization of GdFeCo at fast timescales: injection of a picosecond-wide electrical current pulse[82]. Calculations revealed that the switching energy needed for a ~9 ps electrical pulse to switch a 20 nm^3 cell is ~4 fJ[82], which is much smaller (comparable) than the energy required in conventional STT-MRAM (SOT-MRAM) and the resulting dynamics is an order of magnitude faster[6,82]. Toggle switching (or HI-AOS) has the drawback that the final magnetic state depends on the previous magnetization state and not simply on an externally controllable stimulus such as the direction of the ps current pulse. Current-induced directional magnetization switching on the other hand has been developed for the last decade, using the STT and SOT effects down to ~50 ps current pulses[38]. Most of the conventional SOT and STT experiments, however, were executed using sub-ns current sources

which limits the switching speed of those devices to sub-ns regime[25,27,29,30,83,84]. Garello *et al.*[27], measured SOT-induced switching with ~200 ps current pulse. Recently, Cai *et al.*[84], demonstrated an ultrafast switching time of ~700 ps, which was measured in a CoGd based SOT device using ~400 ps current pulse in the presence of ~144 mT symmetry breaking in-plane magnetic field. Sala *et al.*[85], reported the time-resolved SOT-induced switching in GdFeCo ferrimagnets using sub-ns current (their smallest pulse width was ~300 ps) pulses. They found a widely distributed switching time characterized by significant activation delays, which limit the total switching speed of their devices. Krizakova *et al.*[26,86], demonstrated sub-ns field-free SOT-induced switching in the presence of an STT current and MTJ bias voltage using ~300 ps current pulses.

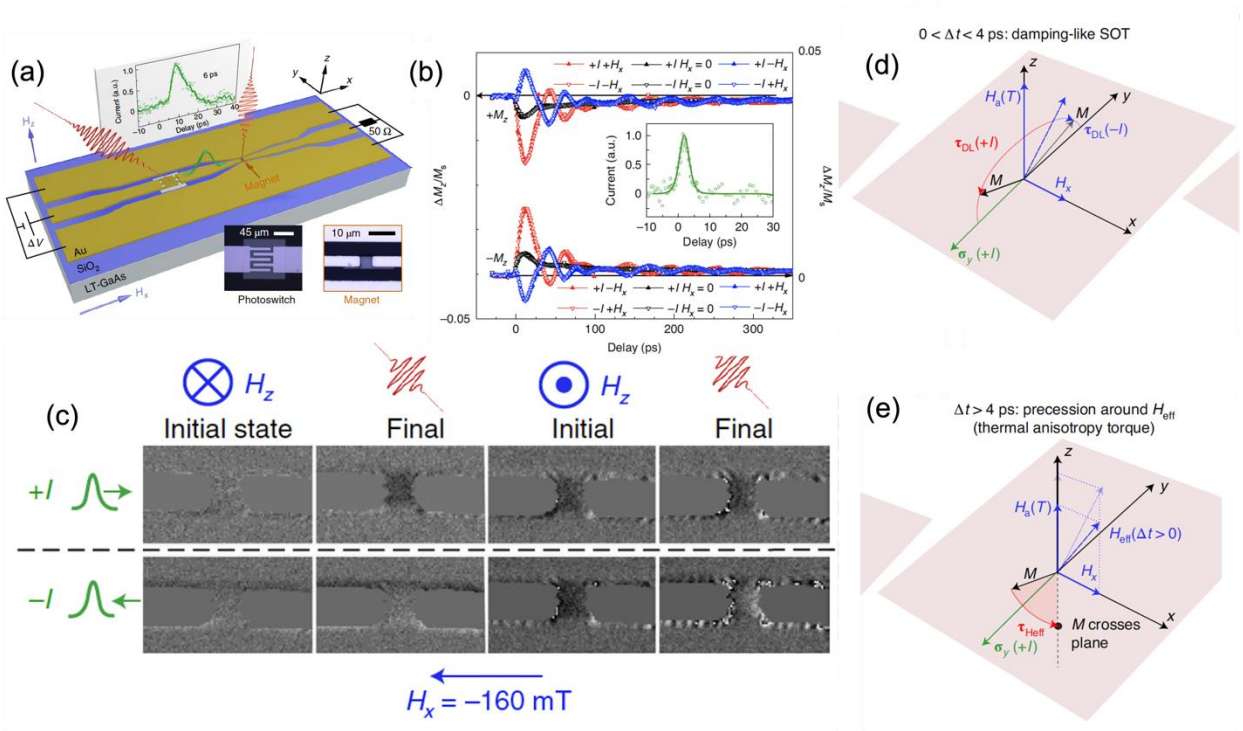


Figure 5: Schematic of the (a) Auston switch which generates ~ 6 ps electrical pulse when exposed to an amplified ultrafast laser pulse as shown by the green line. It also depicts the non-local pump-probe measurement scheme. The optical image of the Auston switch and the magnetic load is shown at the bottom. (b) The magnetization dynamics in the low-fluence limit in the presence of a symmetry-breaking magnetic field. (c) The single-shot MOKE micrograph of the device for successive single-shot laser pulses for different in-plane magnetic fields and ~ps current pulse directions, (d-e) the schematic of the SOT-induced ultrafast reversal mechanism at two different timescales after ultrafast laser excitation. Reproduced with permission from Jhuria *et al.*,[32]. Copyright 2020 Nature Publishing.

In our work[32], we use a ~6 ps electrical pulse generated from an Auston switch to reverse the magnetization of a micro-dot (5x5 μm^2) comprising $Ta_5/Pt_4/Co_1/Cu_1/Ta_4/Pt_1$ stack. The bottom Pt and top Ta layers are used with their opposite spin-Hall angle to enhance the effective spin-orbit torque acting on the Co layer, and the 1 nm thick Cu layer is used to reduce the Dzyaloshinskii–Moriya (DMI) interaction[87] at the top Co

interface and preserve the PMA of Co. From quasi-DC electrical measurements in the Hall-bar geometry, we found that the device switches from $+M_z$ ($-M_z$) to $-M_z$($+M_z$) with 100-microsecond current pulses with a density of 2 x 10^{11} A/m^2) in the presence of an in-plane magnetic field H_x of 160 mT when the current and field directions are parallel (anti-parallel), in agreement with the SOT-induced switching direction expected for the Pt/Co/Ta stack [29,88]. Here $+M_z$ ($-M_z$) is the component of magnetization along its easy axis when a positive (negative) bias field is applied.

We fabricate an Auston switch[82], shown in Fig. 5a, using a LT-GaAs substrate which produces ~6 ps electrical current pulses when excited with 60 fs laser pulses from a 5 kHz repetition rate amplified Ti:sapphire laser. A suitable impedance-matched co-planar waveguide is designed so that the ~ps long electrical pulse can be propagated and delivered to the magnetic load without much distortion. The MOKE micrograph of the device before and after the application of a single electrical pulse is shown in Fig. 5c at a particular in-plane magnetic field for different current directions. It is clear from Fig. 5c that the final magnetization state of the device depends solely on the relative direction of the current pulse (shown in Fig. 5c by the direction of the bias voltage at the Auston switch, for positive bias, current flows along the +x axis) and the in-plane magnetic field (shown in Fig. 5c with the blue arrow). The final magnetization contrast is black (magnetization pointing up from the surface) when the current and in-plane field is opposite and the final magnetization direction is white (magnetization pointing into the surface, highlighted by a red square in Fig. 5c) when the current and in-plane field is parallel. These data confirm that the final magnetization state can be controlled by the external current pulse direction. This is in contrast with our previous observation[82] of toggle-switching of GdFeCo (similar to HI-AOS when exposed to similar ~ps charge current pulses). We calculate the upper bound for the switching energy to be ~50 pJ (for a ~6 ps electrical pulse with current density ~6 x 10^{12} A/m^2) which is in contrast to previous[70,89–94] as well as some recent experiments[21,26,85] where it has been argued that the critical current density (J_c) increases significantly for current pulses-width in sub-ns regime according to $J_C \propto 1/\tau_P$, where τ_P is the current pulse-width. Krizakova *et al.*[26] have studied the reduced magnetic anisotropy (as an immediate effect of Joule heating) as a function of the applied bias voltage across the MTJ and found that the effect of Joule heating increases with increasing device diameter. The elevated electron temperature due to ultrafast heating may reduce the required critical switching energy significantly when compared to the conventional spin-torque induced switching in relatively longer timescales.

In the time-resolved magnetization dynamics shown in Fig. 5b, measured at low-fluence (below the switching threshold), we find ultrafast spin-torque induced coherent oscillations. The sign of the observed oscillations is determined by the direction of the symmetry-breaking field and the injected spin polarization. An in-plane field along the direction parallel (antiparallel) with the injected current causes the moment to precess towards (away from) the initial magnetization direction, causing ΔM_z to decrease (increase) on a

10 ps time- scale. This occurs regardless of the initial up ($+M_z$) or down ($-M_z$) state, as is expected for our SOT stack. We introduce a simple Landau-Liftsitz-Gilbert (LLG) micromagnetic macro-spin simulation incorporating SOT terms to explain the switching dynamics of the system in the presence of the in-plane field which is schematically shown in Fig. 5d-e. According to the model, when the in-plane magnetic field and ps currents are parallel (along +x direction as shown in Fig. 5d), the magnetization is initially at an equilibrium position along the effective magnetic field (H_{eff}), which is a combination of anisotropy field (along the +z axis) and in-plane field (along the +x axis). Now as soon as the current pulse arrives (along the +x axis), a damping-like torque brings the magnetization towards the -y axis and the effective anisotropy reduces due to ultrafast demagnetization. As a result, the direction of H_{eff} changes (as shown in Fig. 5e), the total anisotropy torque reduces, and the magnetization starts to rotate around the new effective magnetic field and ultimately settles down along the switched magnetization direction along -z axis. Although the LLG model does not match the finer details of the early oscillation (between 3 to 25 ps,), particularly in the H_x=0 case, a switching (crossing M_z = 0) as fast as 16 ps is predicted, with ~80% recovery of magnetization expected to be completed in ~50 ps. The discrepancy between the model and the data can possibly be explained by inhomogeneous broadening.

The demonstration of deterministic switching of the out-of-plane magnetized cobalt film by a ~6 ps electrical pulse via SOT opens up an exciting new pathway for ultrafast magnetization switching. Although we use a fs pulse laser triggering an Auston switch in our experiments for convenience, standard nanoscale CMOS transistors have been known to switch on the single ps timescale since the 45 nm technology generation[95] was introduced in 2007, and CMOS switching times are reduced in every subsequent generation. This means that simple CMOS circuits can be used to generate ps duration electrical current pulses capable of triggering ultrafast magnetization switching devices on a chip. Estimates of the minimum current needed to switch a nanoscale magnetic device are well within the range that could be produced using nanoscale CMOS transistors[4,82], thus enabling a highly scalable ultrafast non-volatile magnetic memory bit cell. The observed switching dynamics are found to be mostly governed by damping-like SOT torque acting on demagnetized moments on the ultrafast time scale. The macrospin LLG simulation qualitatively agrees with the experimentally observed magnetization dynamics. Such ps current pulse induced experiments could also be useful in studying inertial dynamics in ferromagnets[96–100] and the resonant dynamics in antiferromagnets[101] which appear in the THz frequency range.

Outlook

In this perspective, we have discussed several recent studies on ultrafast laser-induced switching and ps charge-current induced SOT switching of ferromagnets, which we believe to be a promising route to realize

energy-efficient ultrafast spintronic devices. The RKKY exchange-coupled heterostructure[59,60] ensures zero-crossing of a conventional FM in ~3 ps timescale[60] and thereby stands as a strong candidate to be integrated into MTJ cells for picosecond memory applications. We have modified the existing M3TM model to explain the observed ultrafast switching in such complex structures. A working opto-MTJ cell with relatively high TMR employing an optically switchable FM-FEM heterostructure as the free layer of an MTJ has now been demonstrated[58] with time-resolved magnetization reversal in ~10 ps (for 3 μm diameter memory cell). We have also demonstrated SOT-induced magnetization reversal in a conventional FM using ~6 ps pure charge-current pulses[32]. This approach provides a dramatic expansion of the domain of ultrafast magnetism beyond optically triggered switching to the purely electrical domain.

Two different ultrafast devices have been proposed, namely, the ~ps electrical SOT switching-based MRAM devices and the HI-AOS based opto-spintronic MTJ devices. They each show a promising future to become the alternative technology in the beyond-CMOS era,[2,5,6,11,12] in different applications. They show advantages such as fast switching speed (tens of ps), non-volatility, energy efficiency, and reliable endurance which find applications in logic and memory devices[15,28], stochastic computing[9], ultrafast data transfer etc[1–3,24]. The ps-MRAM devices are likely to be designed as SOT-MRAM structures while the HI-AOS based opto-spintronic MTJ devices could be used as a toggle STT-MRAM structure with much faster switching dynamics. We have already discussed the challenges associated with SOT and STT-based MRAM briefly in the introduction. One of the concerns common to virtually all SOT-MRAM implementations (not just our ps variety) is the requirement of the in-plane symmetry-breaking magnetic field which poses serious challenges in terms of device integration. Different mechanisms like structural asymmetry, in-built in-plane field, strain-induced effects, additional MTJ bias voltage, and STT current are being studied as an alternative to an external in-plane magnetic field[26,83,86,93,102–107]. Novel materials with much higher SOT efficiency (for more energy-efficient SOT switching) have already been studied however, they are not yet easily integrable in a device[5,84,108]. It remains a topic of future research to determine which of these are adaptable to ps SOT.

The ultrafast laser-induced toggle-switchable HI-AOS phenomenon is already being explored and integrated into MTJ cells which offers enhanced energy efficiency and much faster switching compared to conventional MRAM devices[58]. Applications for this technology will likely involve integration with silicon photonics. Kimel *et al.*[11] proposed an interesting idea about switching individual memory cells optically with the assistance of electrical heating by combining fabricated optical waveguides and transistor selectors. An issue with toggle-switching is the requirement of prior knowledge of the magnetization state to switch it to a particular direction. Recently, van Hees *et al.*[52] demonstrated an interesting approach to deterministically switch the magnetization of a Co/Gd ML using two simultaneous ultrafast laser pulses with slightly different pulse energies. So far, we have only discussed about the write current amplitudes

and the writing speed, however for a working device, reading speed and reading error rate are equally important, which depend on the TMR ratio of the device[109]. Increasing the read current amplitude, on one hand, decreases the read sensing error and decreases the read access time, but on the other hand, increases the read disturbance error. Currently, read times are in general engineered to be a few ns for a reasonable read current amplitude[4,110–112]. With the abundance of spintronics-based research around the world focusing on both fundamental understanding and technological developments, we may expect to overcome the hurdles and possibly implement a new generation of high-speed spintronics technology to address the ever-increasing technological and computation needs.

Acknowledgement

This work was supported by ASCENT, one of six centers in JUMP, a Semiconductor Research Corporation (SRC) program also sponsored by DARPA (instrumentation and data acquisition). This work was also supported by the Director, Office of Science, Office of Basic Energy Sciences, Materials Sciences and Engineering Division, of the U.S. Department of Energy under Contract No. DE-AC02-05-CH11231 within the Nonequilibrium Magnetic Materials Program (MSMAG) (theoretical analysis). We also acknowledge support by the National Science Foundation Center for Energy Efficient Electronics Science (instrumentation and data acquisition).

References

[1] S. Bhatti, R. Sbiaa, A. Hirohata, H. Ohno, S. Fukami, and S.N. Piramanayagam, Mater. Today **20**, 530 (2017).

[2] A. Hirohata, K. Yamada, Y. Nakatani, L. Prejbeanu, B. Diény, P. Pirro, and B. Hillebrands, J. Magn. Magn. Mater. **509**, 166711 (2020).

[3] P. Barla, V.K. Joshi, and S. Bhat, J. Comput. Electron. **20**, 805 (2021).

[4] T. Na, S.H. Kang, and S.-O. Jung, IEEE Trans. Circuits Syst. II Express Briefs **68**, 12 (2021).

[5] Q. Shao, P. Li, L. Liu, H. Yang, S. Fukami, A. Razavi, H. Wu, K. Wang, F. Freimuth, Y. Mokrousov, M.D. Stiles, A. Hoffmann, J. Åkerman, K. Roy, S.-H. Yang, K. Garello, and W. Zhang, IEEE Trans. Magn. **57**, 1 (2021).

[6] A. El-Ghazaly, J. Gorchon, R.B. Wilson, A. Pattabi, and J. Bokor, J. Magn. Magn. Mater. **502**, 166478 (2020).

[7] H. Ohno, J. Appl. Phys. **113**, 136509 (2013).

[8] B.N. Engel, J. Akerman, B. Butcher, R.W. Dave, M. DeHerrera, M. Durlam, G. Grynkewich, J. Janesky, S. V Pietambaram, N.D. Rizzo, J.M. Slaughter, K. Smith, J.J. Sun, and S. Tehrani, IEEE Trans. Magn. **41**, 132 (2005).

[9] Z. Guo, J. Yin, Y. Bai, D. Zhu, K. Shi, G. Wang, K. Cao, and W. Zhao, Proc. IEEE **109**, 1398 (2021).

[10] F. Hellman, A. Hoffmann, Y. Tserkovnyak, G.S.D. Beach, E.E. Fullerton, C. Leighton, A.H. MacDonald, D.C. Ralph, D.A. Arena, H.A. Dürr, P. Fischer, J. Grollier, J.P. Heremans, T. Jungwirth, A. V Kimel, B. Koopmans, I.N. Krivorotov, S.J. May, A.K. Petford-Long, J.M. Rondinelli, N. Samarth, I.K. Schuller, A.N. Slavin, M.D. Stiles, O. Tchernyshyov, A. Thiaville, and B.L. Zink, Rev. Mod. Phys. **89**, 1 (2017).

[11] A. V. Kimel and M. Li, Nat. Rev. Mater. **4**, 189 (2019).

[12] E.Y. Vedmedenko, R.K. Kawakami, D.D. Sheka, P. Gambardella, A. Kirilyuk, A. Hirohata, C. Binek, O. Chubykalo-Fesenko, S. Sanvito, B.J. Kirby, J. Grollier, K. Everschor-Sitte, T. Kampfrath, C.Y. You, and A. Berger, J. Phys. D. Appl. Phys. **53**, 453001 (2020).

[13] G. Hu, J.J. Nowak, M.G. Gottwald, S.L. Brown, B. Doris, C.P. D'Emic, P. Hashemi, D. Houssameddine, Q. He, and D. Kim, in *2019 IEEE Int. Electron Devices Meet.* (IEEE, 2019), pp. 2–6.

[14] E.R.J. Edwards, G. Hu, S.L. Brown, C.P. D'Emic, M.G. Gottwald, P. Hashemi, H. Jung, J. Kim, G. Lauer, and J.J. Nowak, in *2020 IEEE Int. Electron Devices Meet.* (IEEE, 2020), p. 24.

[15] K. Garello, F. Yasin, H. Hody, S. Couet, L. Souriau, S.H. Sharifi, J. Swerts, R. Carpenter, S. Rao, and W. Kim, in *2019 Symp. VLSI Circuits* (IEEE, 2019), pp. T194–T195.

[16] S. Ikegawa, F.B. Mancoff, J. Janesky, and S. Aggarwal, IEEE Trans. Electron Devices **67**, 1407 (2020).

[17] S. Aggarwal, H. Almasi, M. DeHerrera, B. Hughes, S. Ikegawa, J. Janesky, H.K. Lee, H. Lu, F.B. Mancoff, K. Nagel, G. Shimon, J.J. Sun, T. Andre, and S.M. Alam, in *2019 IEEE Int. Electron Devices Meet.* (2019), pp. 2.1.1-2.1.4.

[18] V.B. Naik, K. Yamane, T.Y. Lee, J. Kwon, R. Chao, J.H. Lim, N.L. Chung, B. Behin-Aein, L.Y. Hau, D. Zeng, Y. Otani, C. Chiang, Y. Huang, L. Pu, S.H. Jang, W.P. Neo, H. Dixit, S.K.L.C. Goh, E.H. Toh, T. Ling, J. Hwang, J.W. Ting, R. Low, L. Zhang, C.G. Lee, N. Balasankaran, F. Tan, K.W. Gan, H. Yoon, G. Congedo, J. Mueller, B. Pfefferling, O. Kallensee, A. Vogel, V. Kriegerstein, T. Merbeth, C.S. Seet, S. Ong, J. Xu, J. Wong, Y.S. You, S.T. Woo, T.H. Chan, E. Quek, and S.Y. Siah, in *2020 IEEE Int. Electron Devices Meet.* (2020), pp. 11.3.1-11.3.4.

[19] K. Lee, J.H. Bak, Y.J. Kim, C.K. Kim, A. Antonyan, D.H. Chang, S.H. Hwang, G.W. Lee, N.Y. Ji, W.J. Kim, J.H. Lee, B.J. Bae, J.H. Park, I.H. Kim, B.Y. Seo, S.H. Han, Y. Ji, H.T. Jung, S.O. Park, O.I. Kwon, J.W. Kye, Y.D. Kim, S.W. Pae, Y.J. Song, G.T. Jeong, K.H. Hwang, G.H. Koh, H.K. Kang, and E.S. Jung, in *2019 IEEE Int. Electron Devices Meet.* (2019), pp. 2.2.1-2.2.4.

[20] Y. Cao, G. Xing, H. Lin, N. Zhang, H. Zheng, and K. Wang, IScience 101614 (2020).

[21] E. Grimaldi, V. Krizakova, G. Sala, F. Yasin, S. Couet, G. Sankar Kar, K. Garello, and P. Gambardella, Nat. Nanotechnol. **15**, 111 (2020).

[22] V.M. Edelstein, State Commun. **73**, 233 (1990).

[23] A. Manchon, J. Železný, I.M. Miron, T. Jungwirth, J. Sinova, A. Thiaville, K. Garello, and P. Gambardella, Rev. Mod. Phys. **91**, 035004 (2019).

[24] A. Manchon, H.C. Koo, J. Nitta, S.M. Frolov, and R.A. Duine, Nat. Mater. **14**, 871 (2015).

[25] I.M. Miron, K. Garello, G. Gaudin, P.J. Zermatten, M. V. Costache, S. Auffret, S. Bandiera, B. Rodmacq, A. Schuhl, and P. Gambardella, Nature **476**, 189 (2011).

[26] V. Krizakova, E. Grimaldi, K. Garello, G. Sala, S. Couet, G.S. Kar, and P. Gambardella, Phys. Rev. Appl. **15**, 054055 (2021).

[27] K. Garello, C.O. Avci, I.M. Miron, M. Baumgartner, A. Ghosh, S. Auffret, O. Boulle, G. Gaudin, and P. Gambardella, Appl. Phys. Lett. **105**, 212402 (2014).

[28] M. Cubukcu, O. Boulle, N. Mikuszeit, C. Hamelin, T. Bracher, N. Lamard, M.C. Cyrille, L. Buda-Prejbeanu, K. Garello, I.M. Miron, O. Klein, G. De Loubens, V. V. Naletov, J. Langer, B. Ocker, P. Gambardella, and G. Gaudin, IEEE Trans. Magn. **54**, 1 (2018).

[29] M. Baumgartner, K. Garello, J. Mendil, C.O. Avci, E. Grimaldi, C. Murer, J. Feng, M. Gabureac, C. Stamm, Y. Acremann, S. Finizio, S. Wintz, J. Raabe, and P. Gambardella, Nat. Nanotechnol. **12**, 980 (2017).

[30] M.M. Decker, M.S. Wörnle, A. Meisinger, M. Vogel, H.S. Körner, G.Y. Shi, C. Song, M. Kronseder, and C.H. Back, Phys. Rev. Lett. **118**, 257201 (2017).

[31] Y. Jungbum, L. Seo-Won, K.J. Hyun, L.J. Min, S. Jaesung, Q. Xuepeng, L. Kyung-Jin, and Y. Hyunsoo, Sci. Adv. **3**, e1603099 (2021).

[32] K. Jhuria, J. Hohlfeld, A. Pattabi, E. Martin, A.Y. Arriola Córdova, X. Shi, R. Lo Conte, S. Petit-Watelot, J.C. Rojas-Sanchez, G. Malinowski, S. Mangin, A. Lemaître, M. Hehn, J. Bokor, R.B. Wilson, and J. Gorchon, Nat. Electron. **3**, 680 (2020).

[33] P.M. Haney, H.W. Lee, K.J. Lee, A. Manchon, and M.D. Stiles, Phys. Rev. B - Condens. Matter Mater. Phys. **87**, (2013).

[34] B. Koopmans, J.J.M. Ruigrok, F. Dalla Longa, and W.J.M. De Jonge, Phys. Rev. Lett. **95**, 267207 (2005).

[35] A. Barman, S. Wang, O. Hellwig, A. Berger, E.E. Fullerton, and H. Schmidt, J. Appl. Phys. **101**, 09D102 (2007).

[36] S. Pal, D. Polley, R.K. Mitra, and A. Barman, Solid State Commun. **221**, (2015).

[37] A. Barman, S. Mondal, S. Sahoo, and A. De, J. Appl. Phys. **128**, 170901 (2020).

[38] O.J. Lee, D.C. Ralph, and R.A. Buhrman, Appl. Phys. Lett. **99**, 102507 (2011).

[39] E. Beaurepaire, J.-. C. Merle, A. Daunois, and J.-. Y. Bigot, Phys. Rev. Lett. **76**, 4250 (1996).

[40] I. Radu, K. Vahaplar, C. Stamm, T. Kachel, N. Pontius, H.A. Dürr, T.A. Ostler, J. Barker, R.F.L. Evans, R.W. Chantrell, A. Tsukamoto, A. Itoh, A. Kirilyuk, T. Rasing, and A. V. Kimel, Nature **472**, 205 (2011).

[41] T.A. Ostler, J. Barker, R.F.L. Evans, R.W. Chantrell, U. Atxitia, O. Chubykalo-Fesenko, S. El Moussaoui, L. Le Guyader, E. Mengotti, L.J. Heyderman, F. Nolting, A. Tsukamoto, A. Itoh, D. Afanasiev, B.A. Ivanov, A.M. Kalashnikova, K. Vahaplar, J. Mentink, A. Kirilyuk, T. Rasing, and A. V. Kimel, Nat. Commun. **3**, 666 (2012).

[42] I. Radu, C. Stamm, A. Eschenlohr, F. Radu, R. Abrudan, K. Vahaplar, T. Kachel, N. Pontius, R. Mitzner, K. Holldack, and A. Föhlisch, Spin **5**, 1550004 (2015).

[43] M. Beens, M.L.M. Lalieu, A.J.M. Deenen, R.A. Duine, and B. Koopmans, Phys. Rev. B **100**, 220409 (2019).

[44] T.D. Cornelissen, R. Córdoba, and B. Koopmans, Appl. Phys. Lett. **108**, (2016).

[45] A. Ceballos, A. Pattabi, A. El-Ghazaly, S. Ruta, C.P. Simon, R.F.L. Evans, T. Ostler, R.W. Chantrell, E. Kennedy, M. Scott, J. Bokor, and F. Hellman, Phys. Rev. B **103**, 024438 (2021).

[46] L. Le Guyader, M. Savoini, S. El Moussaoui, M. Buzzi, A. Tsukamoto, A. Itoh, A. Kirilyuk, T. Rasing, A. V Kimel, and F. Nolting, Nat. Commun. **6**, 5839 (2015).

[47] M. Beens, M.L.M. Lalieu, R.A. Duine, and B. Koopmans, AIP Adv. **9**, 125133 (2019).

[48] A. El-Ghazaly, B. Tran, A. Ceballos, C.H. Lambert, A. Pattabi, S. Salahuddin, F. Hellman, and J. Bokor, Appl. Phys. Lett. **114**, 232407 (2019).

[49] M.J.G. Peeters, Y.M. van Ballegooie, and B. Koopmans, ArXiv:2105.13862 (2021).

[50] F. Jakobs, T. Ostler, C.-H. Lambert, Y. Yang, S. Salahuddin, R.B. Wilson, J. Gorchon, J. Bokor, and U. Atxitia, Phys. Rev. B **103**, 104422 (2021).

[51] C.S. Davies, T. Janssen, J.H. Mentink, A. Tsukamoto, A. V. Kimel, A.F.G. Van Der Meer, A. Stupakiewicz, and A. Kirilyuk, Phys. Rev. Appl. **13**, 024064 (2020).

[52] Y.L.W. van Hees, P. van de Meugheuvel, B. Koopmans, and R. Lavrijsen, Nat. Commun. **11**, 3835 (2020).

[53] C. Banerjee, N. Teichert, K.E. Siewierska, Z. Gercsi, G.Y.P. Atcheson, P. Stamenov, K. Rode, J.M.D. Coey, and J. Besbas, Nat. Commun. **11**, 1 (2020).

[54] L. Avilés-Félix, L. Álvaro-Gómez, G. Li, C.S. Davies, A. Olivier, M. Rubio-Roy, S. Auffret, A. Kirilyuk, A. V. Kimel, T. Rasing, L.D. Buda-Prejbeanu, R.C. Sousa, B. Dieny, and I.L. Prejbeanu, AIP Adv. **9**, 125328 (2019).

[55] L. Avilés-Félix, A. Olivier, G. Li, C.S. Davies, L. Alvaro-Gómez, M. Rubio-Roy, S. Auffret, A. Kirilyuk, A. V Kimel, T. Rasing, L.D. Buda-Prejbeanu, R.C. Sousa, and I.L. Prejbeanu, Sci. Rep. **10**, 1 (2020).

[56] L. Avilés-Félix, L. Farcis, Z. Jin, L. Álvaro-Gómez, G. Li, K.T. Yamada, A. Kirilyuk, A.V. Kimel, T. Rasing, B. Dieny, and R.C. Sousa, Sci. Rep. **1**, 1 (2021).

[57] J.Y. Chen, L. He, J.P. Wang, and M. Li, Phys. Rev. Appl. **7**, 021001 (2017).

[58] L. Wang, H. Cheng, P. Li, Y. Liu, Y.L.W. Van Hees, R. Lavrijsen, X. Lin, K. Cao, B. Koopmans, and W. Zhao, ArXiv:2011.03612 (2021).

[59] J. Gorchon, C.-H. Lambert, Y. Yang, A. Pattabi, R.B. Wilson, S. Salahuddin, and J. Bokor, Appl. Phys. Lett. **111**, 42401 (2017).

[60] J. Chatterjee, D. Polley, A. Pattabi, H. Jang, S. Salahuddin, and J. Bokor, To Be Publ. (2021).

[61] S. Iihama, Y. Xu, M. Deb, G. Malinowski, M. Hehn, J. Gorchon, E.E. Fullerton, and S. Mangin, Adv. Mater. **30**,

1804004 (2018).

[62] J. Igarashi, Q. Remy, S. Iihama, G. Malinowski, M. Hehn, J. Gorchon, J. Hohlfeld, S. Fukami, H. Ohno, and S. Mangin, Nano Lett. **20**, 8654 (2020).

[63] Q. Remy, J. Igarashi, S. Iihama, G. Malinowski, M. Hehn, J. Gorchon, J. Hohlfeld, S. Fukami, H. Ohno, and S. Mangin, Adv. Sci. **7**, 2001996 (2020).

[64] B. Koopmans, G. Malinowski, F. Dalla Longa, D. Steiauf, M. Fähnle, T. Roth, M. Cinchetti, and M. Aeschlimann, Nat. Mater. **9**, 259 (2010).

[65] A.J. Schellekens and B. Koopmans, Phys. Rev. B - Condens. Matter Mater. Phys. **87**, 020407 (2013).

[66] M.A. Ruderman and C. Kittel, Phys. Rev. **96**, 99 (1954).

[67] T. Kasuy, Prog. Theor. Phys. **16**, 45 (1956).

[68] F.W. Smith, H.Q. Le, V. Diadiuk, M.A. Hollis, A.R. Calawa, S. Gupta, M. Frankel, D.R. Dykaar, G.A. Mourou, and T.Y. Hsiang, Appl. Phys. Lett. **54**, 890 (1989).

[69] N. Nishimura, T. Hirai, A. Koganei, T. Ikeda, K. Okano, Y. Sekiguchi, and Y. Osada, J. Appl. Phys. **91**, 5246 (2002).

[70] S. Ikeda, K. Miura, H. Yamamoto, K. Mizunuma, H.D. Gan, M. Endo, S. Kanai, J. Hayakawa, F. Matsukura, and H. Ohno, Nat. Mater. **9**, 721 (2010).

[71] J. Song, H. DIxit, B. Behin-Aein, C.H. Kim, and W. Taylor, IEEE Trans. Magn. **56**, (2020).

[72] M. Hofherr, P. Maldonado, O. Schmitt, M. Berritta, U. Bierbrauer, S. Sadashivaiah, A.J. Schellekens, B. Koopmans, D. Steil, M. Cinchetti, B. Stadtmüller, P.M. Oppeneer, S. Mathias, and M. Aeschlimann, Phys. Rev. B **96**, 100403 (2017).

[73] A.J. Schellekens, K.C. Kuiper, R.R.J.C. de Wit, and B. Koopmans, Nat. Commun. **5**, 4333 (2014).

[74] M. Beens, R.A. Duine, and B. Koopmans, **102**, 1054442 (2020).

[75] S.S.P. Parkin, Phys. Rev. Lett. **67**, 3598 (1991).

[76] C. Banerjee, K. Rode, G. Atcheson, S. Lenne, P. Stamenov, J.M.D. Coey, and J. Besbas, Phys. Rev. Lett. **126**, 177202 (2021).

[77] C.-M. Lee, L.-X. Ye, T.-H. Hsieh, C.-Y. Huang, and T.-H. Wu, J. Appl. Phys. **107**, 09C712 (2010).

[78] K. Ueda, A.J. Tan, and G.S.D. Beach, AIP Adv. **8**, 125204 (2018).

[79] L. Wang, Y.L.W. van Hees, R. Lavrijsen, W. Zhao, and B. Koopmans, Appl. Phys. Lett. **117**, 022408 (2020).

[80] J. Gorchon, R.B. Wilson, Y. Yang, A. Pattabi, J.Y. Chen, L. He, J.P. Wang, M. Li, and J. Bokor, Phys. Rev. B **94**, (2016).

[81] P.B. Corkum, F. Brunel, N.K. Sherman, and T. Srinivasan-Rao, Phys. Rev. Lett. **61**, 2886 (1988).

[82] Y. Yang, R.B. Wilson, J. Gorchon, C.-H. Lambert, S. Salahuddin, and J. Bokor, Sci. Adv. **3**, e1603117 (2017).

[83] F. Büttner, I. Lemesh, M. Schneider, B. Pfau, C.M. Günther, P. Hessing, J. Geilhufe, L. Caretta, D. Engel, B. Krüger, J. Viefhaus, S. Eisebitt, and G.S.D. Beach, Nat. Nanotechnol. **12**, 1040 (2017).

[84] K. Cai, Z. Zhu, J.M. Lee, R. Mishra, L. Ren, S.D. Pollard, P. He, G. Liang, K.L. Teo, and H. Yang, Nat. Electron. **3**, 37 (2020).

[85] G. Sala, V. Krizakova, E. Grimaldi, C.-H. Lambert, T. Devolder, and P. Gambardella, Nat. Commun. **12**, 656

(2021).

[86] V. Krizakova, K. Garello, E. Grimaldi, G.S. Kar, and P. Gambardella, Appl. Phys. Lett. **116**, 232406 (2020).

[87] S. Woo, K. Litzius, B. Krüger, M.Y. Im, L. Caretta, K. Richter, M. Mann, A. Krone, R.M. Reeve, M. Weigand, P. Agrawal, I. Lemesh, M.A. Mawass, P. Fischer, M. Kläui, and G.S.D. Beach, Nat. Mater. **15**, 501 (2016).

[88] L. Liu, C.-F. Pai, Y. Li, H.W. Tseng, D.C. Ralph, and R.A. Buhrman, **336**, (2012).

[89] J.Z. Sun, R.P. Robertazzi, J. Nowak, P.L. Trouilloud, G. Hu, D.W. Abraham, M.C. Gaidis, S.L. Brown, E.J. O'Sullivan, W.J. Gallagher, and D.C. Worledge, Phys. Rev. B **84**, 064413 (2011).

[90] H. Zhao, B. Glass, P.K. Amiri, A. Lyle, Y. Zhang, Y.-J. Chen, G. Rowlands, P. Upadhyaya, Z. Zeng, J.A. Katine, J. Langer, K. Galatsis, H. Jiang, K.L. Wang, I.N. Krivorotov, and J.-P. Wang, J. Phys. D. Appl. Phys. **45**, 025001 (2012).

[91] D.C. Worledge, G. Hu, D.W. Abraham, J.Z. Sun, P.L. Trouilloud, J. Nowak, S. Brown, M.C. Gaidis, E.J. O'Sullivan, and R.P. Robertazzi, Appl. Phys. Lett. **98**, 022501 (2011).

[92] M. Gajek, J.J. Nowak, J.Z. Sun, P.L. Trouilloud, E.J. O'Sullivan, D.W. Abraham, M.C. Gaidis, G. Hu, S. Brown, Y. Zhu, R.P. Robertazzi, W.J. Gallagher, and D.C. Worledge, Appl. Phys. Lett. **100**, 132408 (2012).

[93] S. V. Aradhya, G.E. Rowlands, J. Oh, D.C. Ralph, and R.A. Buhrman, Nano Lett. **16**, 5987 (2016).

[94] N. Sato, F. Xue, R.M. White, C. Bi, and S.X. Wang, Nat. Electron. **1**, 508 (2018).

[95] K. Mistry, C. Allen, C. Auth, B. Beattie, D. Bergstrom, M. Bost, M. Brazier, M. Buehler, A. Cappellani, R. Chau, C.H. Choi, G. Ding, K. Fischer, T. Ghani, R. Grover, W. Han, D. Hanken, M. Hattendorf, J. He, J. Hicks, R. Huessner, D. Ingerly, P. Jain, R. James, L. Jong, S. Joshi, C. Kenyon, K. Kuhn, K. Lee, H. Liu, J. Maiz, B. McIntyre, P. Moon, J. Neirynck, S. Pae, C. Parker, D. Parsons, C. Prasad, L. Pipes, M. Prince, P. Rarade, T. Reynolds, J. Sandford, L. Shifren, J. Sebastian, J. Seiple, D. Simon, S. Sivakumar, P. Smith, C. Thomas, T. Troeger, P. Vandervoorn, S. Williams, and K. Zawadzki, in *Tech. Dig. - Int. Electron Devices Meet. IEDM* (2007), pp. 247–250.

[96] J.-E. Wegrowe and M.-C. Ciornei, Am. J. Phys. **80**, 607 (2012).

[97] D. Polley, M. Pancaldi, M. Hudl, P. Vavassori, S. Urazhdin, and S. Bonetti, J. Phys. D. Appl. Phys. **51**, 084001 (2018).

[98] K. Neeraj, N. Awari, S. Kovalev, D. Polley, N. Zhou Hagström, S.S.P.K. Arekapudi, A. Semisalova, K. Lenz, B. Green, J.-C. Deinert, I. Ilyakov, M. Chen, M. Bawatna, V. Scalera, M. D'Aquino, C. Serpico, O. Hellwig, J.-E. Wegrowe, M. Gensch, and S. Bonetti, Nat. Phys. **17**, 245 (2020).

[99] R. Mondal, S. Großenbach, L. Rózsa, and U. Nowak, Phys. Rev. B **103**, 104404 (2021).

[100] R. Mondal, M. Berritta, and P.M. Oppeneer, Phys. Rev. B **98**, 214429 (2018).

[101] V. Baltz, A. Manchon, M. Tsoi, T. Moriyama, T. Ono, and Y. Tserkovnyak, Rev. Mod. Phys. **90**, 015005 (2018).

[102] C. Bi, H. Almasi, K. Price, T. Newhouse-Illige, M. Xu, S.R. Allen, X. Fan, and W. Wang, (n.d.).

[103] Z. Zheng, Y. Zhang, V. Lopez-Dominguez, L. Sánchez-Tejerina, J. Shi, X. Feng, L. Chen, Z. Wang, Z. Zhang, K. Zhang, H. Bin, Y. Xu, Y. Zhang, M. Carpentieri, A. Fert, G. Finocchio, W. Zhao, and P. Khalili Amiri, *Field-Free Spin-Orbit Torque-Induced Switching of Perpendicular Magnetization in a Ferrimagnetic Layer with Vertical Composition Gradient* (n.d.).

[104] I.S. Camara, J.-Y. Duquesne, A. Lemaître, C. Gourdon, and L. Thevenard, Phys. Rev. Appl. **11**, 014045 (2019).

[105] M. Natsui, A. Tamakoshi, H. Honjo, T. Watanabe, T. Nasuno, C. Zhang, T. Tanigawa, H. Inoue, M. Niwa, and T. Yoshiduka, in *2020 IEEE Symp. VLSI Circuits* (IEEE, 2020), pp. 1–2.

[106] T. Simsek, IEEE Magn. Lett. **12**, 1 (2021).

[107] C. Zhang, Y. Takeuchi, S. Fukami, and H. Ohno, Appl. Phys. Lett. **118**, 092406 (2021).

[108] S. Liang, S. Shi, C.-H. Hsu, K. Cai, Y. Wang, P. He, Y. Wu, V.M. Pereira, and H. Yang, Adv. Mater. **32**, 2002799 (2020).

[109] J.-Y. Choi, D. Lee, J.-U. Baek, and J.-G. Park, Sci. Rep. **8**, 2139 (2018).

[110] S. Huda and A. Sheikholeslami, IEEE Trans. Circuits Syst. I Regul. Pap. **60**, 1534 (2013).

[111] R. Bishnoi, M. Ebrahimi, F. Oboril, and M.B. Tahoori, in *2014 Int. Test Conf.* (2014), pp. 1–7.

[112] Y. Zhang, A Statistical STT-RAM Design View and Robust Designs at Scaled Technologies, University of Pittsburgh, 2017.